frontiers | Frontiers in Astronomy and Space Sciences

TYPE Original Research
PUBLISHED 07 November 2023
DOI 10.3389/fspas.2023.1274760

OPEN ACCESS

EDITED BY
Rudolf A. Treumann,
Ludwig Maximilian University of Munich, Germany

REVIEWED BY
Xiaochen Shen,
Boston University, United States
Meng Zhou,
Nanchang University, China

*CORRESPONDENCE
J. Joseph,
jayasri-joseph@uiowa.edu

RECEIVED 08 August 2023
ACCEPTED 09 October 2023
PUBLISHED 07 November 2023

CITATION
Joseph J, Jaynes AN, Kurth WS, Menietti JD, Connerney JEP and Bolton SJ (2023), Electron cyclotron harmonic waves in Jovian magnetosphere as seen by Juno. *Front. Astron. Space Sci.* 10:1274760. doi: 10.3389/fspas.2023.1274760

Electron cyclotron harmonic waves in Jovian magnetosphere as seen by Juno

J. Joseph[1]*, A. N. Jaynes[1], W. S. Kurth[1], J. D. Menietti[1], J. E. P. Connerney[2] and S. J. Bolton[3]

[1]Department of Physics and Astronomy, University of Iowa, Iowa City, IA, United States, [2]Goddard Space Flight Center, Greenbelt, MD, United States, [3]Southwest Research Institute, San Antonio, TX, United States

Electron cyclotron harmonic (ECH) waves along with whistler mode waves are suggested to be responsible for causing the persistent diffuse aurora in Jupiter. In this work, for the first time we systematically analyze the ECH waves in the Jovian inner magnetosphere, which was surveyed by Juno during the later orbits (>25). We find that in the Jovian inner magnetosphere, ECH waves occur in two specific regions—one equatorial and the other off-equatorial, just outside the Io torus. Equatorial ECH waves have higher intensity compared to their off-equatorial counterpart. We also notice an overlap between the region of mid-latitude hot injections and the region of off-equatorial ECH wave occurrence. Finally, we show an event to describe the complex nature of ECH wave growth/damping varying with particle density structures of the injection region at mid-latitude.

KEYWORDS

electron cyclotron harmonic waves, electron injection, wave-particle interaction, spin modulation, Jovian magnetosphere

1 Introduction

Electron cyclotron harmonic (ECH) waves (also known as electron Bernstein mode waves) are banded electrostatic emissions, where the wave power peaks at frequencies between the harmonics of electron cyclotron frequency (f_{ce}). Typically wave powers are concentrated at half integer times the electron cyclotron frequencies, i.e., (n + 0.5) f_{ce} for n = 1, 2, 3, *etc.* (Kennel et al., 1970; Shaw and Gurnett, 1975; Meredith et al., 2009). These electrostatic emissions can contribute to the generation of diffuse aurora by energization and pitch angle scattering of electrons with energies in the range from a few hundred eV to a few keV (Thorne, 1983; Horne and Thorne, 1998; Ni et al., 2012; Zhang et al., 2015). Statistical studies on Earth (Meredith et al., 2000; 2009; Ni et al., 2011) show that following geomagnetically disturbed conditions, intense ECH waves are observed in the equatorial (±3°) region just outside the plasmasphere (4 < L < 7), at magnetic local times from 2100 to 0600, approximately 20% of the time. Similar studies at Saturn (Menietti et al., 2017; Long et al., 2021) have also shown a high occurrence rate of ECH waves near the magnetic equators in the night and dawn sectors. However, ECH waves are also observed at mid latitudes (~20°–40°) at Saturn (Long et al., 2021). Equatorial confinement of ECH waves is due to the fact that the convection of plasma from the tail region mainly happens through the plasma sheet containing the thermal plasma (Kennel and Petschek, 1966; Barbosa et al., 1980; Baumjohann, 1993; Ma et al., 2021). On Earth large amplitude ECH waves are often seen in synchronism with particle injections and dipolarization fronts, which modifies the density and temperature ratios between cold and hot electrons

(Angelopoulos et al., 1992; Meredith et al., 1999; Zhang and Angelopoulos, 2014). In rapidly rotating magnetospheres like Saturn and Jupiter internally driven convection (Hill et al., 1981) plays a major role and injections are often observed at higher latitudes (Burch et al., 2005). ECH waves at higher latitudes may extend the pathlength for electrons to interact with the waves, enhancing scattering.

The first observation of ECH waves at Jupiter was recorded during the Voyager flybys (Kurth et al., 1980). Subsequently Galileo observed strong ECH emissions (Menietti et al., 2012) in the low-latitude region of the Jovian middle magnetosphere ($r > 10\ R_J$, where R_J (71,492 km) is the equatorial radius of Jupiter). However, due to the near equatorial nature of Galileo's orbit, information from higher latitudes in the middle magnetosphere was unavailable. In this study, we use wave and particle data from the Juno satellite, which has larger latitudinal coverage of the Jovian middle magnetosphere ($5 < r < 18\ R_J$).

For the first time our study reveals that, like Saturn, Jupiter has two distinct regions of ECH wave occurrence. We further show that the region of ECH wave occurrence at mid latitudes coincides with the region of hot electron injections reported by Kurth et al. (2023). Finally, we reveal the complex nature of ECH wave growth/extinction using an event with simultaneous wave and particle observations.

2 Instrument

The Waves instrument (Kurth et al., 2017) on board Juno is used in this study to obtain the electric and magnetic field measurements. The front-end of the Waves instrument is comprised of one electric dipole antenna, which is sensitive to electric fields parallel to the *y*-axis of the satellite, and one magnetic search coil, which is sensitive to magnetic fields parallel to the spacecraft spin (z) axis. Low frequency electric signals (50 Hz–150 kHz) and magnetic signals (50 Hz–20 kHz) are handled by a low frequency receiver (LFR). The LFR consists of three channels - two of them measure electric fields in the frequency ranges of 50 Hz to 20 kHz and 10–150 kHz, and a third one measures magnetic fields in the range of 50 Hz to 20 kHz. Even though the fractional spectral resolution ($\Delta f/f$) is approximately constant throughout the range of frequencies, the absolute spectral resolution for the 10–150 kHz channel is substantially less than that of the lower band. Data from the LFR is used for the current study. The Waves instrument also has a high frequency receiver (HFR), which covers the frequency range of 0.1–40 MHz. However, sensitivity of the HFR is not sufficient to be used in this study. Apart from the Waves instrument, we also use measurements from the fluxgate magnetometer, which is included in the MAG instrument (Connerney et al., 2017) for measuring the three axis (x, y, and z) background magnetic field. Particle data from the JADE instrument (McComas et al., 2017), specifically the JADE-E sensors that measure electrons in the energy range of ~0.001–100 keV, are used to confirm the correlations between ECH waves and the underlying electron density structure.

Ephemeris information, including the M-shell, MLat and MLT are calculated with 1 minute time resolution by mapping the spacecraft position on the JRM-33 dipole magnetic field model (Connerney et al., 2021) with the magnetodisc model (Connerney et al., 2020).

We encounter several orbit/instrument limitations, which are listed below, for the current study of ECH waves in Jupiter's middle magnetosphere.

1. While our study includes data from Orbit 1 onward, due to precession of the orbital trajectory, only during later orbits (>25), does Juno spend substantial time in the equatorial regions of the middle magnetosphere (<18).
2. Juno did not sample the equatorial region of the middle magnetosphere during day magnetic local times (MLT).
3. Due to the high magnetic field strength of Jupiter, the electron cyclotron frequency (f_{ce}) is large—for example, at R_J = 9.75 and Mlat = 13.3°, f_{ce} = 13.7 kHz. As the study of ECH waves involves multiples of f_{ce}, the required frequencies tend to fall outside the low band (<20 kHz) of the LFR instrument's frequency range in which both electric and magnetic waves are measured. Even though we have electric field measurements above 20 kHz, frequency resolution of the mid band (>20 kHz) LFR instrument is substantially reduced.
4. Due to the lack of 3-axis measurements of the electric and the magnetic vectors, complete wave propagation parameters cannot be determined.
5. Due to high levels of penetrating radiation, limited particle data is available in some regions of the magnetosphere.

3 Observations

Juno Waves data from PJ1 (2016-08-25) to PJ45 (2022-10-02) were used in this study to examine the occurrence of ECH waves in the middle magnetosphere (M < 18) of Jupiter. ECH waves are primarily characterized by bands of raised intensity in E-field between harmonics of f_{ce}. Ideally E/cB also needs to be evaluated to verify the electrostatic nature of these waves. Full characterization of the propagation characteristics of the waves could provide additional confirmation. However, with the limitation of instrumentation on Juno, validation of all of the above criteria for identifying ECH waves is not possible. The problem becomes evident near the planet due to the increase in background magnetic field, which results in large f_{ce}. Since ECH waves are related to harmonics of f_{ce}, measurement of E and B fields at high frequencies are needed. Even though B field measurements may seem unnecessary for identification of ECH waves, any presence of B field would disqualify the emission as ECH waves. The Waves instrument on Juno has reasonable electric and magnetic field measurements up to 20 kHz, beyond which the E-field is measured at a lower resolution and no B-field data are available. So, to cope with these limitations, we mainly rely on the identification of the banded structure in the E-field intensity. Juno Waves instrument records power spectral densities (PSDs) of electric and magnetic fields at incremental frequency intervals (Δf), where $\Delta f/f$ is approximately constant. Using these values, our algorithm first calculates the PSDs between harmonics of f_{ce}, which is determined from the measurement of the background B field (FGM instrument). Then the algorithm identifies events, where the first band (3/2) PSD is greater than 30 times the background PSD and the second band (5/2) PSD is greater than 5 times the

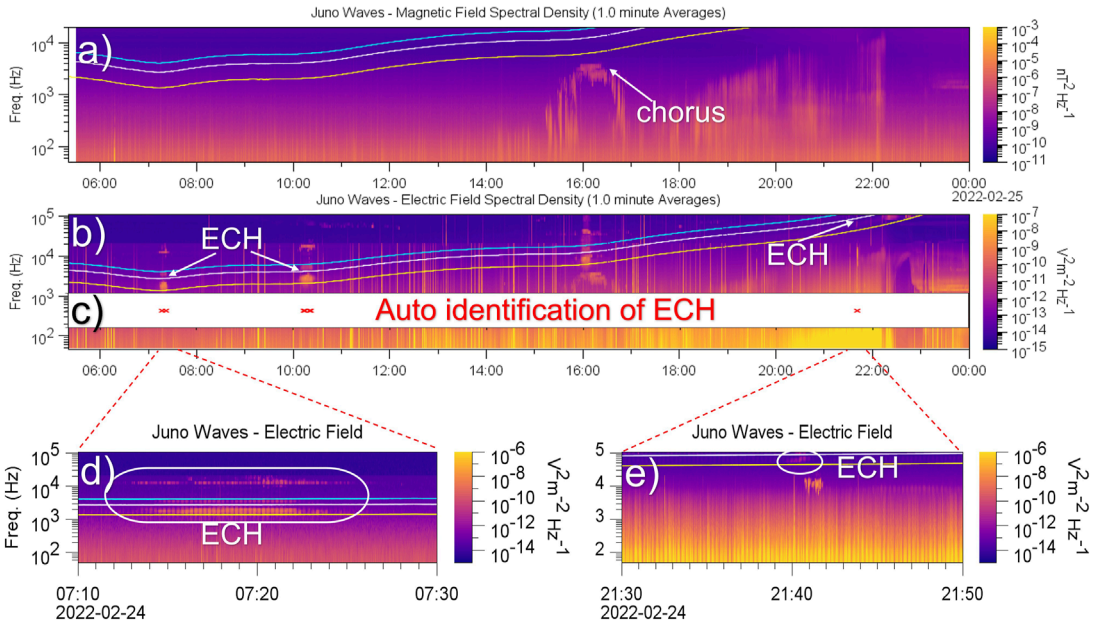

FIGURE 1
An example of algorithmic detection of ECH waves. Panels **(A)** and **(B)** show the power spectral densities (PSDs) of the magnetic field and electric field respectively. On Panel **(C)**, the red markers show the regions of ECH waves detected by the algorithm. Panel **(C)** is overlaid on panel **(B)** for easy comparison. Panels **(D)** and **(E)** are the zoomed in views of two of the ECH wave regions shown in panel **(B)**. Yellow, white, and magenta traces on the plots indicate values of f_{ce}, $2f_{ce}$, and $3f_{ce}$ respectively.

background PSD. We do not track higher harmonics (>5/2) in this study, nor the lone occurrence of the 3/2 band. The in-band PSDs are calculated by integrating the PSDs from n*f_{ce} to (n+1)*f_{ce}, where n = 1 for the first band and n = 2 for the second band, and dividing by the number of frequency bins (Δf) present in the interval (n*f_{ce} - (n+1)*f_{ce}). Due to variation in background noise, background PSDs are separately evaluated for the two bands for each event from the PSDs at the lower boundary of the band, i.e., at f_{ce} and $2f_{ce}$ for the 3/2 and the 5/2 band respectively. Even though the primary process deals with the PSDs of electric field, a similar auxiliary process is executed for PSDs of the magnetic field, too. For frequencies below 20 kHz, the auxiliary process verifies the absence of concurrent magnetic field components. But above 20 kHz, we rely solely on the electric field measurements. An event is registered when within the duration of a minute the PSD of electric field of the 3/2 band is greater than 30 times the background PSD with no corresponding magnetic field and the PSD of electric field of the 5/2 band is greater than 5 times the background PSD. Multiple short duration ECH wave occurrences within a minute are treated as single event. We likely have omitted some ECH occurrences in the vicinity of the planet, where 3/2 or 5/2 band falls above 150 kHz. It is to be noted that the HFR instrument (0.1–40 MHz) is unsuitable for this study due to low frequency resolution and poor sensitivity. Stringent thresholds were used by the algorithm to specifically exclude the ECH-like thermal emission (Sentman, 1982) at high latitudes. Regions of ECH waves with moderate PSDs are often seen surrounding the strong events identified by our algorithm. Weak ECH waves do not affect the particle acceleration, hence eliminating them from the catalog is considered acceptable. Figure 1 shows an example of the auto-detected ECH waves.

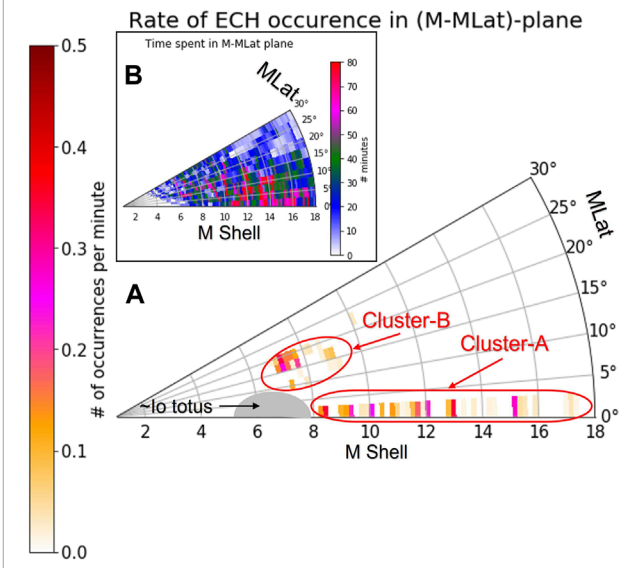

FIGURE 2
Rate of ECH waves occurence in the M-MLat plane. Panel **(A)** shows the ECH wave occurrence rate per minute. ECH waves are concentrated in two regions indicated by Cluster-A and Cluster-B outside the Io plasma torus, whose approximate cross section is shown. Panel **(B)** shows the time spent by Juno at each location.

The occurrence of ECH waves is sorted in magnetic coordinates (M, MLat) according to the JRM33 magnetic field model (Connerney et al., 2021) and the magnetodisc model (Connerney et al., 2020). Identified ECH waves are shown in

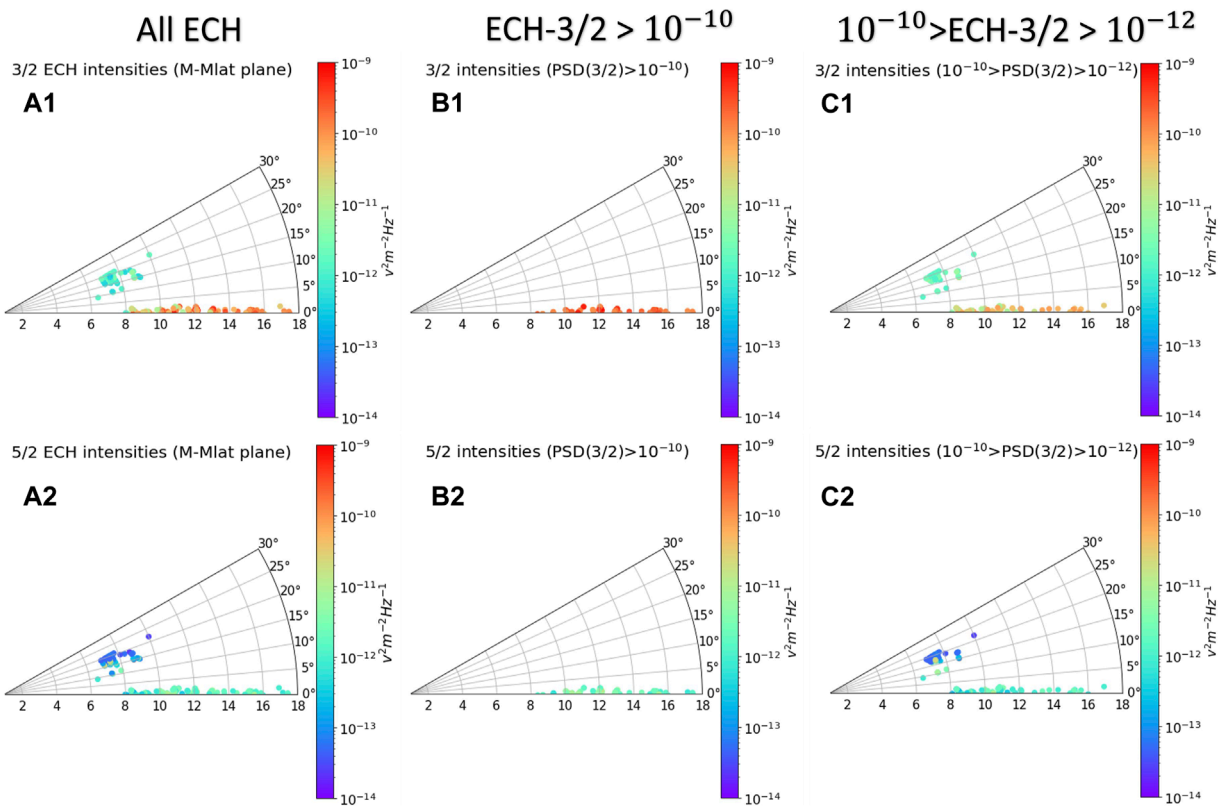

FIGURE 3
Power spectral densities (PSDs) of ECH waves for the first two bands in M-MLat plane. Panels **(A1)** and **(A2)** show the PSDs observed in the 3/2 and 5/2 bands respectively. Panels **(B1, B2)** and **(C1, C2)** show cases of strong (>10^{-10}) and weak (<10^{-10}) PSDs of ECH-3/2 (ECH-5/2) separately.

Figure 2A along with the time spent by Juno at each location (Figure 2B) in the M-MLat plane. The bin resolution used is 0.18 × 3° in M-MLat directions. From Figure 2A, two distinct clusters of ECH wave occurrence are seen—one in the equatorial region and the other at the mid latitude region. Due to the limited (~6 h) coverage of MLT in the inner magnetosphere by Juno, this study does not include ECH wave analysis in the M-MLT plane.

4 Analysis

A complete analysis of waves involves both the magnitude of the wave power and direction of its propagation. Further investigation is possible for each band of the ECH waves.

4.1 Amplitude

In this study, we first examine the relative intensities of the 3/2 and 5/2 ECH bands. Secondly, we map the detailed distribution of PSDs of the 3/2 band in different energy ranges.

Figure 3 shows the average PSDs of electric field for the first two harmonic band (ECH-3/2 and ECH-5/2) in the M-MLat plane. Average PSD of ECH-3/2 in the equatorial region is ~$10^{-10}V^2m^{-2}Hz^{-1}$ (Figure 3A1). We also have a cluster of mid-latitude ECH-3/2 emissions with PSD of ~$10^{-12}V^2m^{-2}Hz^{-1}$. ECH-5/2 has substantially weaker PSDs - ~$10^{-11}V^2m^{-2}Hz^{-1}$ and ~$10^{-13}V^2m^{-2}Hz^{-1}$ (Figure 3A2) at the equatorial and the mid-latitude regions respectively. To view the relative behavior of ECH-3/2 and ECH-5/2, we segregate the overall observations (Figure 3A) into two subgroups as shown in Figures 3B, C.

We sort the ECH-3/2 PSDs into four different levels in the range of $10^{-10}V^2m^{-2}Hz^{-1}$ to $10^{-12}V^2m^{-2}Hz^{-1}$, which is shown in Figures 4A–D. It is evident from Figure 4 that the PSDs of ECH-3/2 are generally higher (~ $10^{-10}V^2m^{-2}Hz^{-1}$) in the equatorial region compared to the PSDs in the mid-latitude region (~ $10^{-11}V^2m^{-2}Hz^{-1}$).

4.2 Polarization

Ideally, the full propagation characteristics should be measured to verify the waves as ECH waves. But, due to the absence of 3-axis electric field measurements on Juno, we resort to an indirect method. Instead, we estimate the polarization of the wave electric field with respect to the background magnetic field. The observed electric field by the Juno-Waves instrument is spin modulated due to the rotation of the electric dipole antenna. When the dipole antenna axis coincides with the orientation of the electric signal oscillation, we record the maximum amplitude. Conversely, a minimum amplitude

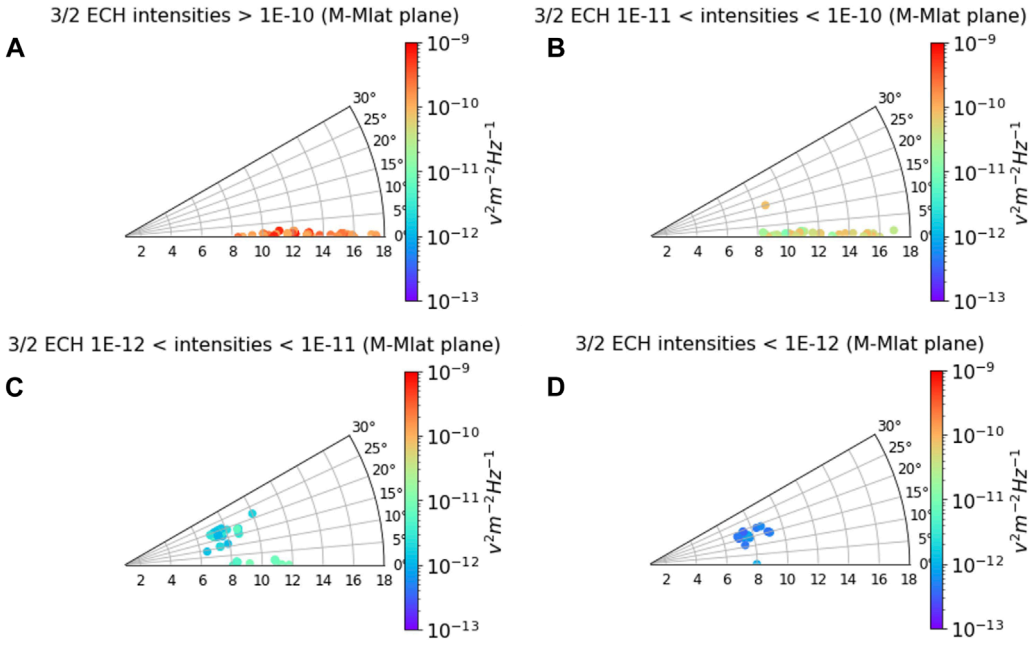

FIGURE 4
Distribution of power spectral density (PSD) of the 3/2-band of ECH waves in M-MLat plane. Panels **(A–D)** shows ECH wave observed within four specific PSD ranges.

is observed when the antenna is perpendicular to the electric field. So, if the ECH wave is perpendicularly polarized as expected, the electric field observed should follow the orientation of the dipole as shown in Figures 5A1, A2. We receive minimum electric field, when the dipole is parallel to the Jovian magnetic field (Figures 5A1, B1, A2, B2) confirming a perpendicularly polarized ECH wave. This is an approximate method.

5 Discussion

This study shows that besides the equatorial region outside the Io torus (cluster-A Figure 2A), ECH waves are seen in the mid latitude region just above the Io torus (cluster-B Figure 2A). At small values of the ratio of the electron plasma frequency to cyclotron frequency $\left(\frac{f_p}{f_{ce}}\right)$, the phase velocity of the waves is high. This condition is favorable for energy diffusion and wave acceleration (Horne and Thorne, 1998; Horne et al., 2003; Gurnett and Bhattacharjee, 2005). $\left(\frac{f_p}{f_{ce}}\right)$ is found to be very high inside the Io torus (Horne et al., 2008). Hence, ECH wave clusters-A and B (Figure 2A) reside just beyond the Io torus. However, it should also be noted that $\left(\frac{f_p}{f_{ce}}\right)\leq 1$ will prohibit the existence of ECH waves as discussed later.

From our analysis, we find that the typical PSDs of mid-latitude ECH waves ($\sim 10^{-11} V^2 m^{-2} Hz^{-1}$) are about an order of magnitude smaller compared to the PSDs of the waves in the equatorial region ($\sim 10^{-10} V^2 m^{-2} Hz^{-1}$). The most important process that scatters inner magnetospheric electrons into the ionosphere is pitch angle diffusion. The pitch angle diffusion coefficient depends on the WNA of the ECH wave (Ni et al., 2012). Even though ECH waves generally have WNA of ~90°, any deviation away from 90° would increase the rate of pitch angle diffusion. We will attempt to estimate the WNA via a detailed analysis of the magnitude of the spin modulation in a future paper.

Generation of ECH waves requires a mixture of cold background plasma and hot plasma. For example, planetward convection of hot plasma sheet electrons from the geomagnetic tail into the cold magnetospheric plasma are expected to generate ECH waves (Kennel et al., 1970). ECH waves are seen at the magnetic equator for most Solar System planets with intrinsic magnetic fields including Earth, Jupiter, Saturn, Uranus and Neptune (Kurth et al., 1980; Kurth et al., 1987; Barbosa et al., 1990; Meredith et al., 2009; Long et al., 2021). Manifestation of these ECH waves is attributed to the increased equatorial plasma density and the equatorial injections of hot plasma in the nightside as a consequence of Dungey/Vasyliunas cycle, which is well studied (Mauk et al., 1999; 2005; Burch et al., 2005). So, here we concentrate on the observation of mid-latitude ECH waves in the Jovian magnetosphere. We see a clear correlation between the regions where injections reported by Kurth et al. (2023) are seen and where the mid latitude ECH waves are observed. ECH wave occurrences are shown in Figure 6B, and injection events are shown in Figure 6A. The shaded background in panels a and b of Figure 6 are the regions where $\left(\frac{f_p}{f_{ce}}\right)$ derived from the models (Divine and Garrett, 1983; Connerney et al., 2017) is less than one. Multiband ECH waves tend to exist in the frequency range between the upper hybrid frequency (f_{UH}) and the electron cyclotron frequency (f_{ce}), when $\left(\frac{f_p}{f_{ce}}\right)<2$ (Gough et al., 1979). The viable frequency range for ECH waves diminishes for $\left(\frac{f_p}{f_{ce}}\right)\leq 1$ as

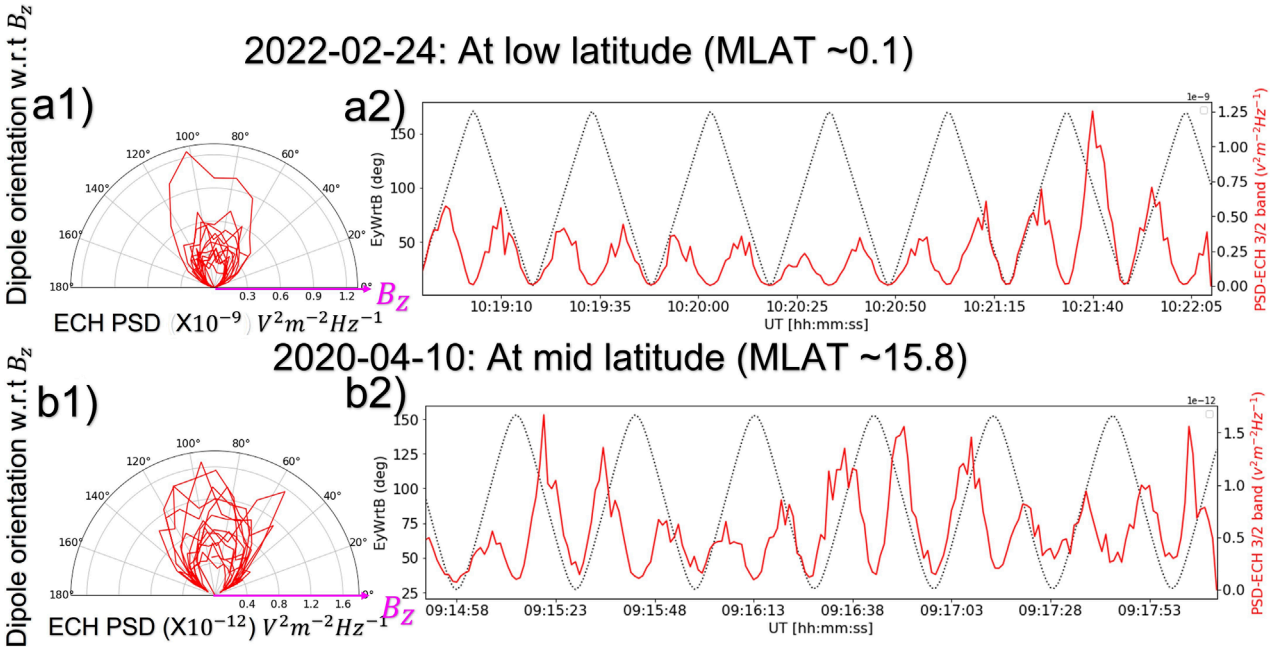

FIGURE 5
Correlation of spin modulated ECH wave PSDs with the dipole antenna orientation. Panels **(A1, B1)** show the electric power received by the dipole as it rotates w.r.t the background magnetic field at low latitudes and at mid latitudes respectively confirming the perpendicular polarization. Panels **(A2, B2)** show the cycle-by-cycle variation revealing the fine structures of alignment between the received signal strength and the dipole direction. The black dotted lines show the dipole orientation as the spacecraft spins. The red lines show the corresponding electric power spectral density (PSD) variation. Note that the electric field is maximum for angles near 90° and minimal for angles closest to 0 and 180°.

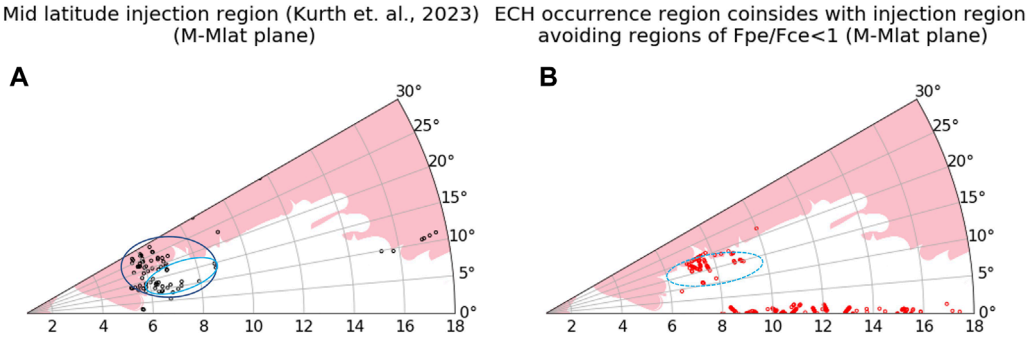

FIGURE 6
Correlations between the injection region and ECH wave occurrence region at mid-latitude in M-MLat plane. Black dots in panel **(A)** shows the locations of injections. Red dots in panel **(B)** shows the locations of ECH waves. Pink shaded areas indicate the regions where $\left(\frac{f_p}{f_{ce}}\right)$ <1.

$f_{uh}^2 = f_p^2 + f_{ce}^2$. So, even though injections are seen irrespective of the value of $\left(\frac{f_p}{f_{ce}}\right)$, ECH waves only exist in the region, where $\left(\frac{f_p}{f_{ce}}\right)$>1(unshaded region of Figure 6A). In other words, parts of the injection region (Figure 6A) that fall within the shaded region do not have a corresponding ECH wave occurrence region (Figure 6B).

Mechanisms that lead to ECH wave intensification in the region of injection may be complex. Generation of ECH waves requires a plasma with two electron populations—a background cold population and a hot population with a loss cone distribution as a free energy source (Ashour-Abdalla and Kennel, 1978a; Horne, 1989; Horne et al., 2003). Parametric studies by Ashour-Abdalla et al. (1979) shows that even though the cold electron density determines the harmonic bands, wave intensification is possible only when the density and temperature ratio between cold and hot electron components are sufficiently small. These conditions are often satisfied in the vicinity of the injection regions and lead to generation and amplification of ECH waves (Zhang and Angelopoulos, 2013). However, excessive modification of the local plasma densities, especially at the fresh injection site may contribute to the extinction of ECH waves. A snapshot of the mid

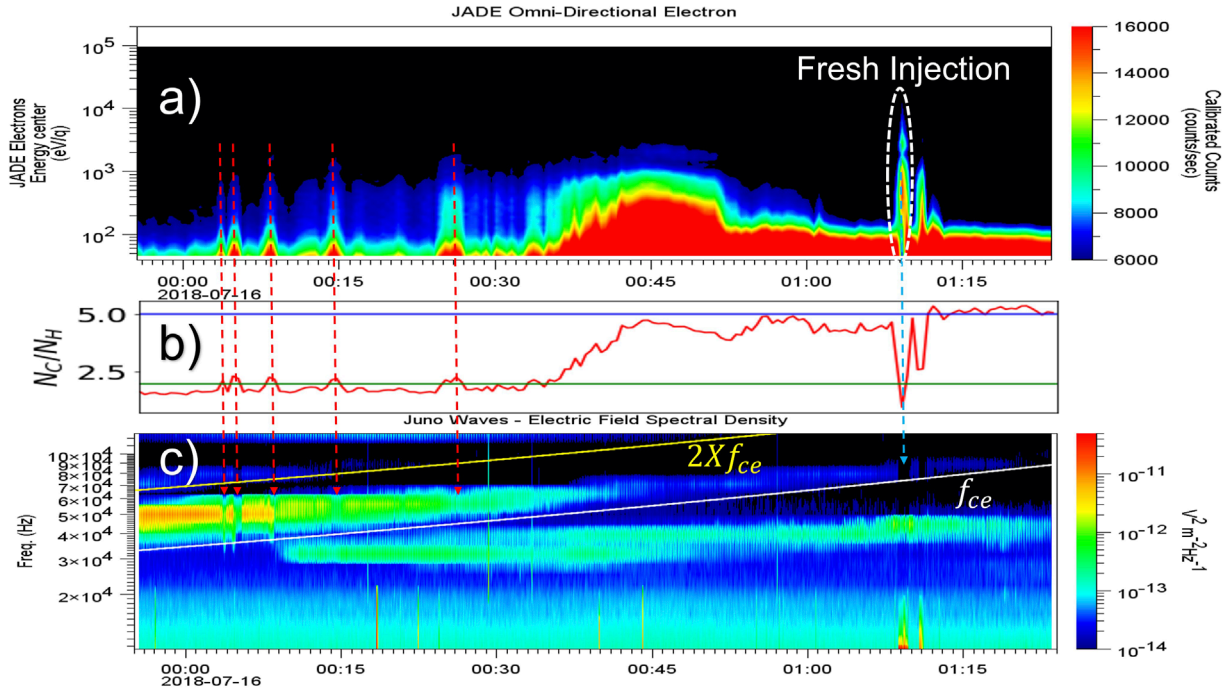

FIGURE 7
An event (PJ-14, 16 July 2018) showing the correlations between the growth/damping of ECH waves and the cold/hot electron density structures in the vicinity of an injection site. Panel **(A)** shows the electron counts at different energy levels. Panel **(B)** shows the ratio of calculated hot to cold electron count. Panel **(C)** shows the electric field power spectral density (PSD). The white and the yellow traces on panel **(C)** represent the values of f_{ce} and $2f_{ce}$ respectively. Red arrows between the panels indicate the regions where sudden changes in cold to hot (N_c/N_h) electron counts resulted in corresponding changes in ECH wave growth. Blue arrow indicates a fresh injection site and the possible disappearance of ECH waves due to lowering of the plasma frequency.

latitude injection region of Jupiter exhibiting such wave-particle behavior is shown in Figure 7. Here, we note that the ECH wave intensifications/extinctions clearly follow the ratio of the cold to hot electron density structures observed by the particle data from JADE in the vicinity of the injection site. A large ratio (>2-5) of cold to hot electron density (N_c/N_h) hampers the growth of ECH waves as shown by Ashour-Abdalla and Kennel (1978b). Electron counts at different energies as observed by JADE is shown in Figure 7A. To approximately estimate the values of N_c/N_h, we set a threshold of 100 eV as a demarcation between cold and hot electrons. Figure 7B shows the variations of the approximated N_c/N_h. PSDs of the ECH waves shown in Figure 7C, tracks the variation of N_c/N_h surprisingly well as shown by the red arrows in the figure. However, the extinction of ECH waves shown by the blue arrow in Figure 7 is likely to be due to drastic reduction in plasma frequency, f_p ($\propto \sqrt{N_c}$), which in turn lowers the upper hybrid frequency to approximately the electron cyclotron frequency. This condition is prevalent in the fresh injection site. This event only gives a glimpse of the complex interplay between the ECH wave growth and underlying plasma properties. It is to be noted that we do not have observational data to show the basic loss cone distribution of the hot electron component for this event. Detailed analysis of the behavior of Jovian ECH waves under different plasma conditions is left for a future study.

6 Conclusion

Key results of this study are listed below.

1. Two distinct regions of ECH wave occurrence are found in the Jovian inner magnetosphere—one at the equator and the other at mid-latitudes.
2. Power spectral densities of equatorial ECH waves are an order of magnitude higher than those of mid-latitude ECH waves.
3. The region of ECH wave occurrence at mid-latitudes coincides with the mid latitude injection region just outside the Io plasma torus.
4. Evidence of ECH wave growth/damping depending on the hot/cold plasma density structure in the mid-latitude injection region is reported.

Juno sampled the middle magnetosphere of Jupiter during limited span of MLTs. We need wave samples for a larger range of MLTs to characterize the MLT dependence of ECH waves distribution. However, the MLT distribution is expected to be like that of Saturn. Also, the trajectory of Juno did not cover the inner magnetosphere of the southern hemisphere well enough to conduct a statistical analysis, even though this is likely to be similar to that of the northern hemisphere.

Data availability statement

Publicly available datasets were analyzed in this study. This data can be found here: Data for Waves instrument, MAG instrument and JADE instrument onboard Juno is taken from https://pds-ppi.igpp.ucla.edu/. Jovian magnetic field models are available at http://lasp.colorado.edu/home/mop/missions/juno/trajectory-information/.

Author contributions

JJ: Conceptualization, Data curation, Formal Analysis, Investigation, Methodology, Software, Validation, Visualization, Writing–original draft. AJ: Funding acquisition, Project administration, Supervision, Writing–review and editing. WK: Data curation, Funding acquisition, Project administration, Supervision, Writing–review and editing. JM: Methodology, Writing–review and editing. JC: Writing–review and editing. SB: Writing–review and editing.

Funding

The author(s) declare financial support was received for the research, authorship, and/or publication of this article. The research at the University of Iowa is supported by NASA through Contract 699041X with the Southwest Research Institute.

Acknowledgments

JJ acknowledges the use of the Space Physics Data Repository at the University of Iowa supported by the Roy J. Carver Charitable Trust.

Conflict of interest

The authors declare that the research was conducted in the absence of any commercial or financial relationships that could be construed as a potential conflict of interest.

Publisher's note

References

Angelopoulos, V., Baumjohann, W., Kennel, C. F., Coronti, F. V., Kivelson, M. G., Pellat, R., et al. (1992). Bursty bulk flows in the inner central plasma sheet. *J. Geophys. Res.* 97, 4027–4039. doi:10.1029/91JA02701

Ashour-Abdalla, M., Kennel, C. F., and Livesey, W. (1979). A parametric study of electron multiharmonic instabilities in the magnetosphere. *J. Geophys. Res.* 84 (A11), 6540–6546. doi:10.1029/JA084iA11p06540

Ashour-Abdalla, M., and Kennel, C. F. (1978b). Multi-harmonic electron cyclotron instabilities. *Geophys. Res. Lett.* 5 (8), 711–714. doi:10.1029/GL005i008p00711

Ashour-Abdalla, M., and Kennel, C. F. (1978a). Nonconvective and convective electron cyclotron harmonic instabilities. *J. Geophys. Res.* 83 (A4), 1531–1543. doi:10.1029/JA083iA04p01531

Barbosa, D. D., Kurth, W. S., Cairns, I. H., Gurnett, D. A., and Poynter, R. L. (1990). Electrostatic electron and ion cyclotron harmonic waves in Neptune's magnetosphere. *Geophys. Res. Lett.* 17, 1657–1660. doi:10.1029/GL017i010p01657

Baumjohann, W. (1993). The near-Earth plasma sheet: an AMPTE/IRM perspective. *Space Sci. Rev.* 64, 141–163. doi:10.1007/BF00819660

Burch, J. L., Goldstein, J., Hill, T. W., Young, D. T., Crary, F. J., Coates, A. J., et al. (2005). Properties of local plasma injections in Saturn's magnetosphere. *Geophys. Res. Lett.* 32, L14S02. doi:10.1029/2005GL022611

Connerney, J. E. P., Benn, M., Bjarno, J. B., Denver, T., Espley, J., Jorgensen, J. L., et al. (2017). The Juno magnetic field investigation. *Space Sci. Rev.* 213, 39–138. doi:10.1007/s11214-017-0334-z

Connerney, J. E. P., Timmins, S., Herceg, M., and Joergensen, J. L. (2020). A Jovian magnetodisc model for the Juno era. *J. Geophys. Res. Space Phys.* 125, e2020JA028138. doi:10.1029/2020JA028138

Connerney, J. E. P., Timmins, S., Oliversen, R. J., Espley, J. R., Joergensen, J. L., Kotsiaros, S., et al. (2021). A new model of Jupiter's magnetic field at the completion of Juno's prime mission. *J. Geophys. Res. Planets* 127 (2), e2021JE007055. doi:10.1029/2021JE007055

Divine, N., and Garrett, H. B. (1983). Charged particle distributions in Jupiter's magnetosphere. *J. Geophys. Res.* 88, 6889–6903. doi:10.1029/JA088iA09p06889

Gough, M. P., Christiansen, P. J., Martelli, G., and Gershuny, E. J. (1979). Interaction of electrostatic waves with warm electrons at the geomagnetic equator. *Nature* 279, 515–517. doi:10.1038/279515a0

Gurnett, D. A., and Bhattacharjee, A. (2005). *Introduction to plasma physics: with space and laboratory applications*. Cambridge, UK: Cambridge University Press, 133–134. doi:10.1017/CBO9780511809125

Hill, T. W., Dessler, A. J., and Maher, L. J. (1981). Corotating magnetospheric convection. *J. Geophys. Res.* 86, 9020–9028. doi:10.1029/JA086iA11p09020

Horne, R. B. (1989). Path-integrated growth of electrostatic waves: the generation of terrestrial myriametric radiation. *J. Geophys. Res.* 94 (A7), 8895–8909. doi:10.1029/JA094iA07p08895

Horne, R. B., Thorne, R. M., Glauert, S. A., Menietti, J. D., Shprits, Y. Y., and Gurnett, D. A. (2008). Gyro-resonant electron acceleration at Jupiter. *Nat. Phys.* 4 (4), 301–304. doi:10.1038/nphys897

Horne, R. B., Thorne, R. M., Meredith, N. P., and Anderson, R. R. (2003). Diffuse auroral electron scattering by electron cyclotron harmonic and whistler mode waves during an isolated substorm. *J. Geophys. Res.* 108 (A7), 1290. doi:10.1029/2002JA009736

Horne, R. B., and Thorne, R. M. (1998). Potential waves for relativistic electron scattering and stochastic acceleration during magnetic storms. *Geophys. Res. Lett.* 25 (15), 3011–3014. doi:10.1029/98GL01002

Kennel, C. F., and Petschek, H. E. (1966). Limit on stably trapped particle fluxes. *J. Geophys. Res.* 71, 1–28. doi:10.1029/JZ071i001p00001

Kennel, C. F., Scarf, F. L., Fredricks, R. W., McGehee, J. H., and Coroniti, F. V. (1970). VLF electric field observations in the magnetosphere. *J. Geophys. Res.* 75 (31), 6136–6152. doi:10.1029/JA075i031p06136

Kurth, W. S., Barbosa, D. D., Gurnett, D. A., and Scarf, F. L. (1980). Electrostatic waves in the Jovian magnetosphere. *Geophys. Res. Lett.* 7 (1), 57–60. doi:10.1029/GL007i001p00057

Kurth, W. S., Barbosa, D. D., Gurnett, D. A., and Scarf, F. L. (1987). Electrostatic waves in the magnetosphere of Uranus. *J. Geophys. Res.* 92, 15225–15233. doi:10.1029/JA092iA13p15225

Kurth, W. S., Hospodarsky, G. B., Faden, J. B., Sulaiman, A. H., Mauk, B. H., Clark, G., et al. (2023). "Evidence of fresh injections related to the interchange instability in the Io torus," in Proceedings of Ninth Planetary, Solar, and Heliospheric Radio Emissions Conference, Dublin, September 2022. doi:10.25546/103104

Kurth, W. S., Hospodarsky, G. B., Kirchner, D. L., Mokrzycki, B. T., Averkamp, T. F., Robison, W. T., et al. (2017). The Juno waves investigation. *Space Sci. Rev.* 213 (1–4), 347–392. doi:10.1007/s11214-017-0396-y

Long, M., Gu, X., Ni, B., Cao, X., Ma, X., and Zhao, Y. (2021). Global distribution of electrostatic electron cyclotron harmonic waves in Saturn's magnetosphere: a survey of over13-year Cassini RPWS observations. *J. Geophys. Res. Planets* 126, e2020JE006800. doi:10.1029/2020JE006800

Ma, Q., Li, W., Zhang, X.-J., Shen, X.-C., Daly, A., Bortnik, J., et al. (2021). Energetic electron distributions near the magnetic equator in the Jovian plasma sheet and outer radiation belt using Juno observations. *Geophys. Res. Lett.* 48, e2021GL095833. doi:10.1029/2021GL095833

Mauk, B. H., Saur, J., Mitchell, D. G., Roelof, E. C., Brandt, P. C., Armstrong, T. P., et al. (2005). Energetic particle injections in Saturn's magnetosphere. *Geophys. Res. Lett.* 32, L14S05. doi:10.1029/2005GL022485

Mauk, B. H., Williams, D. J., McEntire, R. W., Khurana, K. K., and Roederer, J. G. (1999). Storm-like dynamics of Jupiter's inner and middle magnetosphere. *geophys. Res.* 104, 22759–22778. doi:10.1029/1999JA900097

McComas, D. J., Alexander, N., Allegrini, F., Bagenal, F., Beebe, C., Clark, G., et al. (2017). The jovian auroral distributions experiment (JADE) on the Juno mission to jupiter. *Space Sci. Rev.* 213, 547–643. doi:10.1007/s11214-013-9990-9

Menietti, J. D., Averkamp, T. F., Kurth, W. S., Ye, S.-Y., Gurnett, D. A., and Cecconi, B. (2017). Survey of Saturn electrostatic cyclotron harmonic wave intensity. *J. Geophys. Res. Space Phys.* 122, 8214–8227. doi:10.1002/2017JA023929

Menietti, J. D., Shprits, Y. Y., Horne, R. B., Woodfield, E. E., Hospodarsky, G. B., and Gurnett, D. A. (2012). Chorus, ECH, and Z mode emissions observed at Jupiter and Saturn and possible electron acceleration. *J. Geophys. Res.* 117, A12214. doi:10.1029/2012JA018187

Meredith, N. P., Horne, R. B., Johnstone, A. D., and Anderson, R. R. (2000). The temporal evolution of electron distributions and associated wave activity following substorm injections in the inner magnetosphere. *J. Geophys. Res.* 105 (12), 12907–12917. doi:10.1029/2000JA900010

Meredith, N. P., Horne, R. B., Thorne, R. M., and Anderson, R. R. (2009). Survey of upper band chorus and ECH waves: implications for the diffuse aurora. *J. Geophys. Res.* 114, A07218. doi:10.1029/2009JA014230

Meredith, N. P., Johnstone, A. D., Szita, S., Horne, R. B., and Anderson, R. R. (1999). Pancake" electron distributions in the outer radiation belts. *J. Geophys. Res.* 104, A12431–A12444. doi:10.1029/1998JA900083

Ni, B., Liang, J., Thorne, R. M., Angelopoulos, V., Horne, R. B., Kubyshkina, M., et al. (2012). Efficient diffuse auroral electron scattering by electrostatic electron cyclotron harmonic waves in the outer magnetosphere: a detailed case study. *J. Geophys. Res.* 117, A01218. doi:10.1029/2011JA017095

Ni, B., Thorne, R., Liang, J., Angelopoulos, V., Cully, C., Li, W., et al. (2011). Global distribution of electrostatic electron cyclotron harmonic waves observed on THEMIS. *Geophys. Res. Lett.* 38, L17105. doi:10.1029/2011GL048793

Sentman, D. D. (1982). Thermal fluctuations and the diffuse electrostatic emissions. *geophys. Res.* 87, 1455–1472. doi:10.1029/JA087iA03p01455

Shaw, R. R., and Gurnett, D. A. (1975). Electrostatic noise bands associated with the electron gyrofrequency and plasma frequency in the outer magnetosphere. *J. Geophys. Res.* 80 (31), 4259–4271. doi:10.1029/JA080i031p04259

Thorne, R. M. (1983). "Microscopic plasma processes in the Jovian magnetosphere," in *Physics of the jovian magnetosphere*. Editor A. J. Dessler (Cambridge, U. K: Cambridge Univ. Press), 454–488. doi:10.1017/CBO9780511564574.014

Zhang, X.-J., Angelopoulos, V., Ni, B., Thorne, R. M., and Horne, R. B. (2013). Quasi-steady, marginally unstable electron cyclotron harmonic wave amplitudes. *J. Geophys. Res. Space Phys.* 118, 3165–3172. doi:10.1002/jgra.50319

Zhang, X., Angelopoulos, V., Ni, B., and Thorne, R. M. (2015). Predominance of ECH wave contribution to diffuse aurora in Earth's outer magnetosphere. *J. Geophys. Res. Space Phys.* 120, 295–309. doi:10.1002/2014JA020455

Zhang, X., and Angelopoulos, V. (2014). On the relationship of electrostatic cyclotron harmonic emissions with electron injections and dipolarization fronts. *J. Geophys. Res. Space Phys.* 119, 2536–2549. doi:10.1002/2013JA019540